NANO LETTERS

Letter

pubs.acs.org/NanoLett

Direct-Write X-ray Nanopatterning: A Proof of Concept Josephson Device on $Bi_2Sr_2CaCu_2O_{8+\delta}$ Superconducting Oxide

Marco Truccato,*[,†] Angelo Agostino,[‡] Elisa Borfecchia,[‡] Lorenzo Mino,[§] Eleonora Cara,[†] Alessandro Pagliero,[†] Nidhi Adhlakha,[†] Lise Pascale,[‡] Lorenza Operti,[‡] Emanuele Enrico,[§] Natascia De Leo,[§] Matteo Fretto,[§] Gema Martinez-Criado,[∥] and Carlo Lamberti[‡,⊥]

[†]Department of Physics, Interdepartmental Centre NIS, University of Torino, via Giuria 1, I-10125 Torino, Italy

[‡]Department of Chemistry, Interdepartmental Centre NIS and INSTM Centro di Riferimento, University of Torino, via Giuria 7, I-10125 Torino, Italy

[§]INRIM, National Institute for Metrological Research, Strada delle Cacce 91, I-10135 Torino, Italy

[∥]Experiments Division, European Synchrotron Radiation Facility, 71 Avenue des Martyrs, 38000 Grenoble, France

[⊥]Southern Federal University, Zorge Street 5, 344090 Rostov-on-Don, Russia

Supporting Information

ABSTRACT: We describe the first use of a novel photoresist-free X-ray nanopatterning technique to fabricate an electronic device. We have produced a proof-of-concept device consisting of a few Josephson junctions by irradiating microcrystals of the $Bi_2Sr_2CaCu_2O_{8+\delta}$ (Bi-2212) superconducting oxide with a 17.6 keV synchrotron nanobeam. Fully functional devices have been obtained by locally turning the material into a nonsuperconducting state by means of hard X-ray exposure. Nano-XRD patterns reveal that the crystallinity is substantially preserved in the irradiated areas that there is no evidence of macroscopic crystal disruption. Indications are that O ions have been removed from the crystals, which could make this technique interesting also for other oxide materials. Direct-write X-ray nanopatterning represents a promising fabrication method exploiting material/material rather than vacuum/material interfaces, with the potential for nanometric resolution, improved mechanical stability, enhanced depth of patterning, and absence of chemical contamination with respect to traditional lithographic techniques.

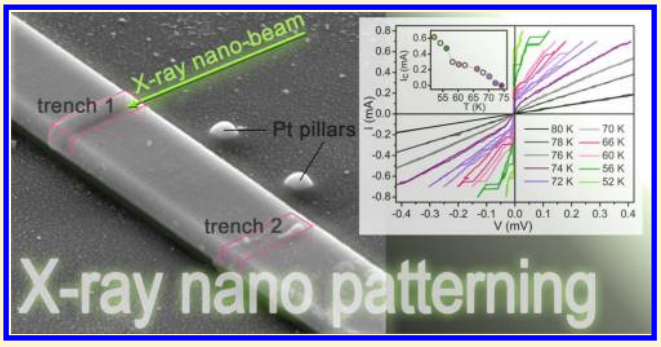

KEYWORDS: *nanopatterning, X-ray nanoprobe, synchrotron radiation, high-temperature superconductors (HTSC), Bi-2212, intrinsic Josephson junctions*

In microelectronics, the minimum feature size has gradually moved from the micro- to the nanodomain, and mass production of processors at the 14 nm technological node has recently started.[1,2] This quest for improved device performance has stimulated the development of several lithographic techniques. In this respect, the success of the approaches based on photolithographic processes has been based on the exploitation of light sources with shorter and shorter wavelengths, down to the 193 nm ArF lasers, representing the present standard for high volume production. At the moment, the use of shorter wavelengths is still the subject of intense research efforts. Extreme ultraviolet (EUV) lithography exploiting λ = 13.5 nm is considered a good candidate for sub-20 nm technological nodes and indeed has already shown the capability to produce patterns with resolutions down to 8 nm half-pitch in its interference version,[3] even though many problems still have to be solved about the power of the light sources[4] and the resist resolution.[5]

Concerning radiation with $\lambda \lesssim 1$ nm (i.e., in the realm of X-rays) remarkable results have been obtained in the field of micromachining by means of the LIGA process.[6] Fully functional static random access memory (SRAM) devices with 250 nm minimum feature size have also been fabricated by X-ray lithography,[7] using the conventional mask-based approach. Due to the fact that mask fabrication is very challenging, maskless methods could represent an interesting alternative. However, lab-scale sources presently show severe limitations in terms of X-ray flux and beam size;[8] therefore, much work has been based on the exploitation of synchrotron radiation sources. For instance, hard X-rays have been proved to promote the growth of ZnO crystallites from sol-gel films obtaining well-defined patterns,[9] and continuous lines with

Received: November 9, 2015
Revised: January 26, 2016
Published: January 27, 2016

DOI: 10.1021/acs.nanolett.5b04568
Nano Lett. 2016, 16, 1669−1674

minimum width of about 25 nm have been directly written in PMMA.[10] Typically, these experiments rely on the use of soft X-rays focused by Fresnel zone plates[11] and are invariably based on the fact that suitably designed polymers or other organic molecules can be locally altered when exposed to large enough X-ray doses, so that they can be selectively removed by a developing solution in order to generate the desired pattern.

Few reports have also shown that synchrotron radiation can directly modify the properties of inorganic materials by displacing light atoms in their crystal structure. For instance, a 100 nm beam of 640 eV photons can create clusters of color centers in LiF with typical sizes of about 500 nm by producing fluorine vacancies.[12] Moreover, it has been demonstrated that irradiation with 8 keV X-rays can induce irreversible modifications in the electrical properties of TiO_2[13] and also a reversible metal−insulator transition at low temperature in a magnetoresistive manganite.[14] However, no electronic device has been fabricated so far by means of this technique. On the other hand, oxide electronics has gained considerable attention in recent years and has demonstrated the possibility to play a significant role as an extension and a complement for the silicon technology. Several materials have been proposed as promising candidates for memory cells with a novel design,[15] and others like indium gallium zinc oxide have been proven to be suitable for the fabrication of small-scale integrated circuits on flexible substrates.[16] These complex oxides exhibit a variety of peculiar physical properties that are of technological interest, like for instance the appearance of giant spin splitting[17] and optically induced magnetization[18] in $SrTiO_3$ (STO), or of a two-dimensional electron liquid at the $LaAlO_3$−$SrTiO_3$ interface.[19]

Among these special properties, superconductivity is of paramount importance because of its several applications. $YBa_2Cu_3O_{7-x}$ (Y-123) and $Bi_2Sr_2CaCu_2O_{8+\delta}$ (Bi-2212) represent two of the most extensively studied superconducting oxides, because of their high critical temperatures $T_c \approx 80-90$ K. They share with STO the key role played by the oxygen nonstoichiometry, which affects both their structural and electronic properties, being able to tune their T_c and even to drive them to a nonsuperconducting state.[20,21] Besides large power applications, they have attracted a lot of interest also in the field of electronics because of their electronic structure, which consists of a stack of superconducting planes separated along their normal direction (i.e., the crystal c axis) by a distance comparable to the corresponding superconducting coherence length ξ_c (for Bi-2212 at $T = 0$, $\xi_c \approx 1$ Å).[22] This favorable situation gives rise to a coupling between the adjacent superconducting planes, originating to the so-called intrinsic Josephson junctions (IJJs),[23] which can be exploited to obtain radiation emission in the THz range.[24] In all of these electronic applications, photolithographic processes have been carried out in a traditional way by means of optical or electron-beam impression of a resist, whose pattern has been subsequently transferred to the material by etching, therefore introducing vacuum/oxide interfaces at some stage of the process to define the device geometry. This procedure has been followed even when the device sizes were critically small, like for instance in the case of Y-123 nanowires intended for photon detection.[25,26] However, it is becoming increasingly clear that a different approach based on X-ray radiation is possible. Indeed, it has recently been shown that irradiating La_2CuO_{4+y} at 12.4 keV can modify its T_c, and it has been hypothesized that this phenomenon could lead to a novel patterning method with a maximum possible resolution of about 6 nm.[27] Nevertheless, no functional electrical device has been produced so far following these speculations.

Recently our group showed that high-dose irradiation at 17 keV can affect both structural and electronic properties of Bi-2212 by modifying its oxygen content.[28] This result has opened a window to the practical realization of a direct hard X-ray patterning method, suggesting that if the X-ray exposure of the material could induce a large enough oxygen depletion to drive it to a nonsuperconducting state, then it would be possible to pattern the desired geometry without using intermediate photoresist-related and etching stages. Here, we present a proof-of-concept device fabricated with a synchrotron radiation nanoprobe by exploiting this novel direct-writing, photoresist-free approach.

The first step in the fabrication is represented by the production of a chip suitable for measuring the electrical properties of Bi-2212 along precisely known crystal directions. For the purpose of this experiment, we have selected Bi-2212 microcrystals with the shape of whiskers because of their geometrical features, well suited for the fabrication of nanodevices, and their nearly perfect single-crystal nature, being free of macroscopic defects in their pristine state.[29] Typical lattice parameters for the Bi-2212 orthorhombic crystal structure are a = 5.397 Å, b = 5.400 Å, and c = 30.56 Å. Whisker-like crystals have the shape of tapes with their edges aligned along the a, b, and c crystal axes, with typical ratios for their sizes of about 1000:10:1 along the a, b, and c axis, respectively (see Figure 1a,d). The crystals were grown starting

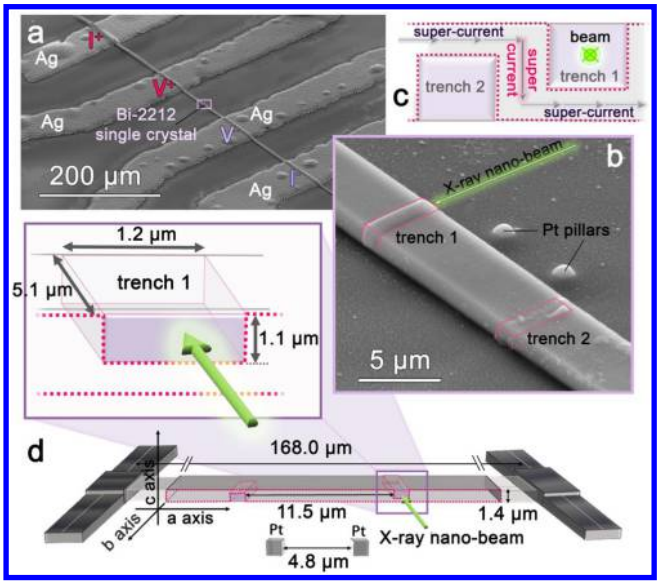

Figure 1. (a) Scanning Electron Microscope (SEM) image of a Bi-2212 microcrystal mounted on the chip for electrical characterization. The current and voltage Ag electrodes used for the four-probe technique are labeled as I^+, I^-, V^+, and V^-, respectively. (b) Magnification of the Bi-2212 microcrystal in the region patterned by X-ray irradiation, located between the voltage contacts. The green arrow represents the X-ray nanobeam, parallel to the [010] direction, employed to write the two trenches highlighted by pink contours. In the image, the two Pt pillars used for alignment are also visible. (c) Schematic of the modifications induced by the trenches in the path of the superconducting current, designed to force it along the c axis across a stack of IJJs. (d) Schematic of the geometry of the device, highlighting the relevant sizes.

DOI: 10.1021/acs.nanolett.5b04568
Nano Lett. 2016, 16, 1669−1674

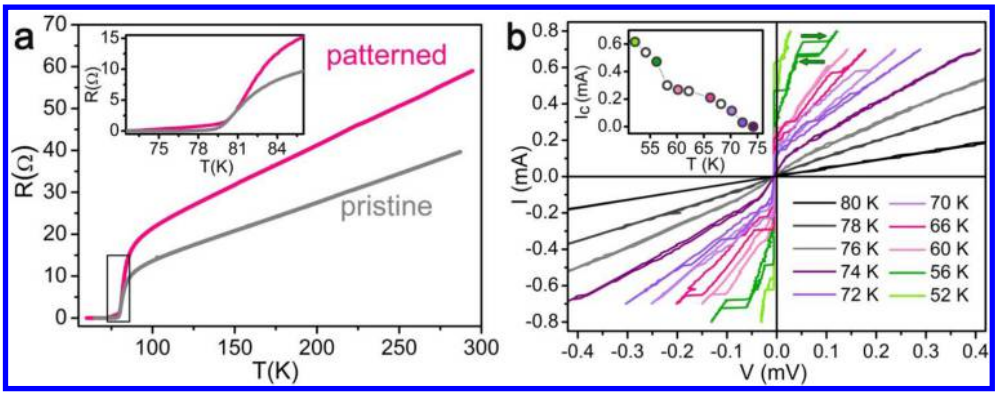

Figure 2. (a) Comparison of the resistance versus temperature behavior measured in the four-probe configuration between pristine and patterned conditions. The inset represents a magnification of the superconducting transition region. (b) $I-V$ characteristics of a patterned device measured at constant temperatures between 52 and 80 K. The green arrows exemplify the typical hysteretic pattern in the case of $T = 56$ K. The inset shows the temperature behavior of the corresponding critical current values I_c. Void circles refer to curves that have not been shown in the main panel for clarity.

from high purity Bi_2O_3, $SrCO_3$, $CaCO_3$, and CuO powders with stoichiometric ratios Bi:Sr:Ca:Cu = 1.5:1:1:2 in controlled temperature and atmosphere conditions.[30] After mechanical selection under an optical microscope, they were mounted onto sapphire substrates with their c axis normal to the substrate plane. Silver stripes 2.5 μm thick were deposited by physical vapor deposition and annealed at 450 °C for 5 min in O_2 to obtain good contact resistances and perform electrical characterization via a standard four-probe method (see Figure 1a). Two Pt pillars about 1 μm high were deposited on the sapphire substrates near the crystals by means of focused ion beam (FIB)-assisted chemical vapor deposition with a FEI Quanta 3D FEG (Nanofacility Piemonte, INRIM) at a Ga-ion current of 10 pA, in order to facilitate the location of the area to be patterned by the X-ray nanobeam (see Figure 1b,d).

For X-ray nanopatterning we employed the intense hard X-ray nanobeam produced at the long canted beamline ID16B at the European Synchrotron Radiation Facility (ESRF). In our experiments, we operated in pink-beam mode, using a double white mirror, and a nanofocusing optics based on Kirkpatrick–Baez mirrors,[31] producing a high photon flux ($1-5 \times 10^{11}$ ph/s) at $E = 17.65$ keV with $\Delta E/E \approx 10^{-2}$. The beam sizes at the focal plane were 57×45 nm^2 (V × H) evaluated by the knife-edge scan method. In order to precisely locate the regions of interest for X-ray nanopatterning inside the Bi-2212 microcrystals, we acquired X-ray fluorescence (XRF) profiles using an energy dispersive Si drift detector placed at $(15 \pm 5)°$ with respect to the sample surface. Then the patterning procedure was performed by raster scanning two regions of the Bi-2212 microcrystals about 1×1 μm^2 in size with the nanobeam parallel to the [010] crystallographic direction, defining two *trenches* in proximity of the Pt pillars. The irradiation time was finely tuned to drive the material into its nonsuperconducting state only in these regions without dramatically perturbing the crystal structure, as it will be discussed in the following. Typical exposure parameters have been about 2 s/point and about 60 nm spacing between adjacent points. Because the length of the irradiated area along the a axis was much greater than the superconducting coherence length in the ab plane ($\xi_{ab}(T = 0) \approx 19$ Å),[22,32,33] the adopted patterning geometry for the two trenches was expected to break the superconducting coupling in the ab planes and therefore to modify the path of the superconducting current, forcing it to flow along the direction where superconductivity survives in the form of Josephson coupling, that is, the c axis. Therefore, a stack of IJJs was expected to be obtained as sketched in Figure 1c, thus reproducing the same structure that is usually obtained by means of Ga-FIB etching.[34]

Electrical characterization was performed in a continuous flow Janis ST-100 helium cryostat in the temperature range $45 \text{ K} \leq T \leq 290$ K. The R vs T behaviors were acquired at a constant current value of 1 μA, whereas for the $I-V$ characteristics the maximum current was set at about 0.8 mA to guarantee device integrity and avoid self-heating phenomena at the current electrodes. The corresponding results for a device patterned by means of this novel procedure are presented in Figure 2. A remarkable increase of about 50% can be observed in the device resistance at any temperature after X-ray exposure, clearly testifying a change in its electrical properties (see Figure 2a). A detailed analysis of the temperature region corresponding to the superconducting transition reveals that the temperature T_c of the inflection point changes from 80.7 K in the pristine state to 81.5 K after the patterning process, that is, beyond the experimental uncertainty of 0.2 K. Moreover, the inset of Figure 2a also shows that the patterning stage modifies the device behavior below T_c, giving rise to a significant tail of nonvanishing resistance values down to about 72 K. Because both the T_c and the resistivity values of Bi-2212 are related to its nonstoichiometric oxygen content,[20,35] these facts indicate that irradiating the trenches has generated some local variation of the structure of the crystal, probably due to oxygen loss. This information can be completed by Figure 2b, where the $I-V$ characteristics of the patterned device are displayed. It can be noticed that, with decreasing the temperature, a zero-voltage branch develops up to the critical current value I_c, above which at least one voltage jump to another resistive branch can be observed. The jumps between the branches are hysteretic, in the sense that at any temperature the current value corresponding to a jump to a more dissipative branch is larger than the one corresponding to a jump to a less resistive branch. It is also worth noticing that the amplitude of the hysteresis (i.e., the difference between these two current values) increases with decreasing the temperature. All of these features correspond to the typical behavior of a stack of underdamped intrinsic Josephson junctions, very similar to what can be observed in Bi-2212 mesas patterned via more conventional methods such as Ar-ion milling or FIB-etching.[36,37] The inset of Figure 2b also shows that I_c increases with decreasing the

DOI: 10.1021/acs.nanolett.5b04568
Nano Lett. 2016, 16, 1669–1674

temperature, as expected, with the value measured at T = 52 K corresponding to a critical current density $J_c \approx 1000$ A cm^{-2}. This value compares favorably to the ones measured in stacks of IJJs made out of the same kind of Bi-2212 microcrystals by means of FIB-etching,[38] indicating that the material providing the IJJs of the device is optimally doped.

By combining the information presented in Figure 2a and b, it is possible to state that the superconducting current has been forced to flow along the c axis because the X-ray irradiation has driven the doping level of the trench regions out of the superconducting regime. According to the results of our previous experiments,[28] this doping change could correspond to a local oxygen depletion that has also increased the normal state resistivity of the irradiated regions, as confirmed by the increase of the total resistance of the device. This interpretation is also supported by the very low value of the threshold displacement energy for interstitial oxygen atoms in Bi-2212, which is of the order of only 2 eV.[39,40] A possible alternative or additional effect could be represented by an increase of the mosaic structure inside the crystal, which could create a series of crystalline subdomains responsible for the resistance variation.

Moreover, the appearance of a nonvanishing resistance tail in the R vs T curve below T_c suggests that the oxygen content has also changed in some region that still remains superconducting. The fact that the tail appears in the same curve whose T_c corresponds to optimal doping indicates that this region is electrically in-series with the stack region, and its shape suggests the possibility that some distribution of depressed T_c' values has been locally generated in the material, with 72 < T_c' < 81.5 K. These features indicate that the oxygen depletion has likely extended slightly beyond the irradiated areas, inducing some gradient in the O content in the 300 nm thick regions just above and below each of the trenches, respectively, where the current is forced to flow across material portions with depressed T_c'.

In order to get a deeper insight about the modifications induced in the irradiated regions, we have also collected a series of nano-XRD patterns in transmission geometry with a FreLoN taper CCD camera. Figure 3a displays a representative pattern collected in the portion of the crystal between the voltage electrodes before trench irradiation. The rings corresponding to thermally evaporated polycrystalline Ag are clearly visible, along with a series of equatorial peaks that can be identified with a (00l) series of the Bi-2212 single crystal, in agreement with our experimental geometry. The same pattern acquisition has been repeated after trench irradiation, both inside and outside one trench, as shown in Figure 3b and c, respectively. The most notable feature is that, though the pattern measured out of the trench is practically undistinguishable from the one recorded before irradiation, a new ring can be detected in the trench, which is compatible with the intense (120) reflection of polycrystalline α-Bi_2O_3. Moreover, the (00l) series of Bi-2212 seems also to be somehow affected, but the use in the present experiment of a pink-beam mode hinders the determination of the c-axis lattice parameter, which is beyond the purpose of the present study.

However, a few very interesting remarks can be done. First, the irradiated regions appear to at least partially retain the single-crystal structure of Bi-2212, while some portion of them is turned into polycrystalline Bi_2O_3. This observation can be interpreted on the basis of the phenomenon already reported by Luo et al.,[41] where oxygen atoms from inner layers of Bi-2212 have been shown to be attracted by metallic adatoms toward the surface BiO layer of the single crystals, giving rise to Bi_2O_3 clusters on top of them. The present results show that an analogous mechanism may take place in our experiment, with its driving force represented by the X-ray irradiation. It is also worth noting that the formation of Bi_2O_3 in the irradiated regions would correspond to the insertion of insulating trenches in the device, because the α-Bi_2O_3 resistivity at 100 K that can be deduced from literature[42] is $\rho_{Bi_2O_3}$(100 K) $\approx 10^{20}$ Ω m, much greater than the corresponding value $\rho_{c,2212}$(100 K) = 4−40 × 10^{-2} Ω m for the c-axis resistivity of Bi-2212.[35] However, in Figure 3b the Bi_2O_3 reflection appears to be less intense than the Bi-2212 series, suggesting that it should represent a minor volume fraction of the trench.

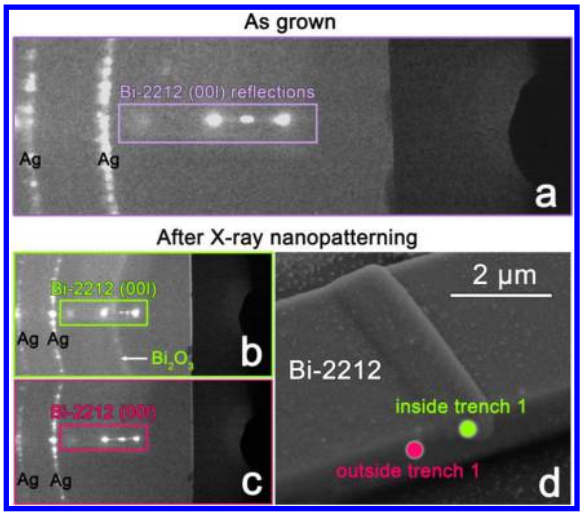

Figure 3. (a) Typical XRD frame acquired before X-ray irradiation. The series of relevant (00l) peaks of Bi-2212 is highlighted, as well as the polycrystalline Ag rings resulting from Ag thermal evaporation to make the electrical contacts. (b) Diffraction pattern observed inside trench 1 after its irradiation. Besides the Bi-2212 (00l) peaks and the Ag rings, the new ring compatible with the formation of Bi_2O_3 is also indicated. (c) Pattern measured after X-ray irradiation out of trench 1. (d) SEM image of trench 1 after X-ray irradiation. The positions where the nano-XRD patterns of panels b and c have been measured are indicated (marker sizes are larger than the real beam size).

Second, it is evident that the trenches can be easily localized by means of SEM analysis because of a local volume expansion induced by the synchrotron radiation, as it can be appreciated in Figure 2d. At least for the c-axis direction, this is in agreement with a crystal oxygen depletion process, which is expected to induce an elongation of the c-axis lattice parameter and therefore an expansion along the direction normal to the substrate.

Our results show that the patterning procedure can already be controlled up to the extent necessary to produce IJJ devices. Besides the photoresist-free approach, the present work is innovative also for the highest photon energy (17.65 keV) ever used for direct write X-ray patterning, and is one of the few reports exploiting Kirkpatrick−Baez mirrors instead of Fresnel zone plates to focus the beam. The reproducibility of the process has been assessed on a second Bi-2212 microcrystal from the same synthesis batch resulting in equivalent device properties (see Figures S1 and S2 of the Supporting Information). The peculiar features of this novel method rely on the use of X-ray radiation to locally modify the crystalline environment and to remove the most loosely bound atoms

DOI: 10.1021/acs.nanolett.5b04568
Nano Lett. 2016, 16, 1669−1674

(typically O in our case) in the material, triggering a completely different electrical behavior. In principle, this idea could be extended to any oxide whose electrical properties critically depend on the O atom content or arrangement. The ultimate space resolution of this technique has still to be determined, but among the possible advantages of this method we can envisage an improved mechanical stability, a higher thermal conductivity of the patterned material, the possibility of performing the patterning process at ambient pressure, and the absence of chemical contamination, especially with respect to the use of Ga-FIB etching. Another interesting feature is represented by fabrication of the pattern by means of the insertion of new material/material interfaces instead of the usual material/vacuum interfaces, which could be exploited to obtain the desired propagation of electromagnetic waves if the dielectric constant of the irradiated regions can be tuned to suitable values. Finally, the high penetration depth of the radiation, which for hard X-rays is of the order of tens of micrometers, could allow patterning thick layers of material with a high aspect ratio, potentially achieving higher fidelity in the pattern transfer because of a higher steepness of the device delimiting surfaces compared to what is obtained by ordinary ion-milling methods.

■ ASSOCIATED CONTENT

Supporting Information

The Supporting Information is available free of charge on the ACS Publications website at DOI: 10.1021/acs.nanolett.5b04568.

Resistance vs temperature behavior and $I-V$ curves of a second IJJ device fabricated by means of direct-write X-ray patterning of another Bi-2212 microcrystal. (PDF)

■ AUTHOR INFORMATION

Corresponding Author

*E-mail: marco.truccato@unito.it.

Notes

The authors declare no competing financial interest.

■ ACKNOWLEDGMENTS

The authors thank the ESRF for the beamtime allocated. They also gratefully acknowledge Compagnia di San Paolo for financial support to NanoFacility Piemonte at INRIM. This work has been carried out under project NANO-X jointly approved and funded by University of Torino and Compagnia di San Paolo. C.L. also acknowledges the Mega-grant of the Russian Federation

■ REFERENCES

(1) Seisyan, R. P. *Tech. Phys.* **2011**, *56*, 1061−1073.
(2) Vaidyanathan, K.; Ng, S. H.; Morris, D.; Lafferty, N.; Liebmann, L.; Bender, M.; Huang, W. B.; Lai, K. F.; Pileggi, L.; Strojwas, A. *Proc. SPIE* **2012**, *8327*, 83270K.
(3) Paivanranta, B.; Langner, A.; Kirk, E.; David, C.; Ekinci, Y. *Nanotechnology* **2011**, *22*, 375302.
(4) Mizoguchi, H.; Nakarai, H.; Abe, T.; Ohta, T.; Nowak, K. M.; Kawasuji, Y.; Tanaka, H.; Watanabe, Y.; Hori, T.; Kodama, T.; Shiraishi, Y.; Yanagida, T.; Yamada, T.; Yamazaki, T.; Okazaki, S.; Saitou, T. Sub-hundred Watt operation demonstration of HVM LPP-EUV Source. In *Extreme Ultraviolet*; Spie-Int Soc Optical Engineering: Bellingham, WA, 2014; Vol. *9048*.
(5) Itani, T.; Kozawa, T. *Jpn. J. Appl. Phys.* **2013**, *52*, 010002.
(6) Ehrfeld, W.; Lehr, H. *Radiat. Phys. Chem.* **1995**, *45*, 349−365.
(7) Viswanathan, R.; Seeger, D.; Bright, A.; Bucelot, T.; Pomerene, A.; Petrillo, K.; Blauner, P.; Agnello, P.; Warlaumont, J.; Conway, J.; Patel, D. *J. Vac. Sci. Technol., B: Microelectron. Process. Phenom.* **1993**, *11*, 2910−2919.
(8) Kalaiselvi, S. M. P.; Tan, T. L.; Talebitaher, A.; Lee, P.; Heussler, S. P.; Breese, M. B. H.; Rawat, R. S. *Phys. Lett. A* **2015**, *379*, 560−569.
(9) Malfatti, L.; Pinna, A.; Enzo, S.; Falcaro, P.; Marmiroli, B.; Innocenzi, P. *J. Synchrotron Radiat.* **2015**, *22*, 165−171.
(10) Leontowich, A. F. G.; Hitchcock, A. P.; Watts, B.; Raabe, J. *Microelectron. Eng.* **2013**, *108*, 5−7.
(11) Lee, S. Y.; Noh, D. Y.; Lee, H. C.; Yu, C. J.; Hwu, Y.; Kang, H. C. *J. Synchrotron Radiat.* **2015**, *22*, 781−785.
(12) Larciprete, R.; Gregoratti, L.; Danailov, M.; Montereali, R. M.; Bonfigli, I.; Kiskinova, M. *Appl. Phys. Lett.* **2002**, *80*, 3862−3864.
(13) Chang, S. H.; Kim, J.; Phatak, C.; D'Aquila, K.; Kim, S. K.; Kim, J.; Song, S. J.; Hwang, C. S.; Eastman, J. A.; Freeland, J. W.; Hong, S. *ACS Nano* **2014**, *8*, 1584−1589.
(14) Kiryukhin, V.; Casa, D.; Hill, J. P.; Keimer, B.; Vigliante, A.; Tomioka, Y.; Tokura, Y. *Nature* **1997**, *386*, 813−815.
(15) Jeong, D. S.; Thomas, R.; Katiyar, R. S.; Scott, J. F.; Kohlstedt, H.; Petraru, A.; Hwang, C. S. *Rep. Prog. Phys.* **2012**, *75*, 076502.
(16) Kim, Y. H.; Heo, J. S.; Kim, T. H.; Park, S.; Yoon, M. H.; Kim, J.; Oh, M. S.; Yi, G. R.; Noh, Y. Y.; Park, S. K. *Nature* **2012**, *489*, 128−U191.
(17) Santander-Syro, A. F.; Fortuna, F.; Bareille, C.; Rodel, T. C.; Landolt, G.; Plumb, N. C.; Dil, J. H.; Radovic, M. *Nat. Mater.* **2014**, *13*, 1085−1090.
(18) Rice, W. D.; Ambwani, P.; Bombeck, M.; Thompson, J. D.; Haugstad, G.; Leighton, C.; Crooker, S. A. *Nat. Mater.* **2014**, *13*, 481−487.
(19) Ohtomo, A.; Hwang, H. Y. *Nature* **2004**, *427*, 423−426.
(20) Triscone, G.; Genoud, J. Y.; Graf, T.; Junod, A.; Muller, J. *Phys. C* **1991**, *176*, 247−256.
(21) Nakazawa, Y.; Ishikawa, M. *Phys. C* **1989**, *158*, 381−384.
(22) Pomar, A.; Ramallo, M. V.; Mosqueira, J.; Torron, C.; Vidal, F. *Phys. Rev. B: Condens. Matter Mater. Phys.* **1996**, *54*, 7470−7480.
(23) Kleiner, R.; Muller, P. *Phys. Rev. B: Condens. Matter Mater. Phys.* **1994**, *49*, 1327−1341.
(24) Ozyuzer, L.; Koshelev, A. E.; Kurter, C.; Gopalsami, N.; Li, Q.; Tachiki, M.; Kadowaki, K.; Yamamoto, T.; Minami, H.; Yamaguchi, H.; Tachiki, T.; Gray, K. E.; Kwok, W. K.; Welp, U. *Science* **2007**, *318*, 1291−1293.
(25) Nawaz, S.; Arpaia, R.; Lombardi, F.; Bauch, T. *Phys. Rev. Lett.* **2013**, *110*, 167004.
(26) Arpaia, R.; Ejrnaes, M.; Parlato, L.; Tafuri, F.; Cristiano, R.; Golubev, D.; Sobolewski, R.; Bauch, T.; Lombardi, F.; Pepe, G. P. *Phys. C* **2015**, *509*, 16−21.
(27) Poccia, N.; Fratini, M.; Ricci, A.; Campi, G.; Barba, L.; Vittorini-Orgeas, A.; Bianconi, G.; Aeppli, G.; Bianconi, A. *Nat. Mater.* **2011**, *10*, 733−736.
(28) Pagliero, A.; Mino, L.; Borfecchia, E.; Truccato, M.; Agostino, A.; Pascale, L.; Enrico, E.; De Leo, N.; Lamberti, C.; Martinez-Criado, G. *Nano Lett.* **2014**, *14*, 1583−1589.
(29) Latyshev, Y. I.; Gorlova, I. G.; Nikitina, A. M.; Antokhina, V. U.; Zybtsev, S. G.; Kukhta, N. P.; Timofeev, V. N. *Phys. C* **1993**, *216*, 471−477.
(30) Truccato, M.; Rinaudo, G.; Manfredotti, C.; Agostino, A.; Benzi, P.; Volpe, P.; Paolini, C.; Olivero, P. *Supercond. Sci. Technol.* **2002**, *15*, 1304−1310.
(31) Martinez-Criado, G.; Borfecchia, E.; Mino, L.; Lamberti, C. Micro and nano X-ray beams. In *Characterization of Semiconductor Heterostructures and Nanostructures*, 2nd ed.; Lamberti, C., Agostini, G., Eds.; Elsevier: Amsterdam, 2013; pp 361−412.
(32) Triscone, G.; Khoder, A. F.; Opagiste, C.; Genoud, J. Y.; Graf, T.; Janod, E.; Tsukamoto, T.; Couach, M.; Junod, A.; Muller, J. *Phys. C* **1994**, *224*, 263−276.
(33) Li, M.; van der Beek, C. J.; Konczykowski, M.; Menovsky, A. A.; Kes, P. H. *Phys. Rev. B: Condens. Matter Mater. Phys.* **2002**, *66*, 66.

DOI: 10.1021/acs.nanolett.5b04568
Nano Lett. 2016, 16, 1669−1674

(34) Kim, S. J.; Yamashita, T.; Nagao, M.; Sato, M.; Maeda, H. *Jpn. J. Appl. Phys. Part 1 - Regul. Pap. Short Notes Rev. Pap.* **2002**, *41*, 4283−4286.
(35) Watanabe, T.; Fujii, T.; Matsuda, A. *Phys. Rev. Lett.* **1997**, *79*, 2113−2116.
(36) Yurgens, A. A. *Supercond. Sci. Technol.* **2000**, *13*, R85−R100.
(37) Latyshev, Y. I.; Yamashita, T.; Bulaevskii, L. N.; Graf, M. J.; Balatsky, A. V.; Maley, M. P. *Phys. Rev. Lett.* **1999**, *82*, 5345−5348.
(38) Inomata, K.; Kawae, T.; Nakajima, K.; Kim, S. J.; Yamashita, T. *Appl. Phys. Lett.* **2003**, *82*, 769−771.
(39) Runde, M.; Routbort, J. L.; Rothman, S. J.; Goretta, K. C.; Mundy, J. N.; Xu, X.; Baker, J. E. *Phys. Rev. B: Condens. Matter Mater. Phys.* **1992**, *45*, 7375−7382.
(40) Pinera, I.; Cruz, C. M.; Abreu, Y.; Leyva, A. *Phys. Status Solidi A* **2007**, *204*, 2279−2286.
(41) Luo, Y. S.; Yang, Y. N.; Weaver, J. H. *Phys. Rev. B: Condens. Matter Mater. Phys.* **1992**, *46*, 1114−1121.
(42) Harwig, H. A.; Gerards, A. G. *J. Solid State Chem.* **1978**, *26*, 265−274.

DOI: 10.1021/acs.nanolett.5b04568
Nano Lett. 2016, 16, 1669−1674